John von Neumann Institute for Computing

Turbulence in Laterally Extended Systems

Jörg Schumacher, Matthias Pütz

published in

Parallel Computing: Architectures, Algorithms and Applications ,
C. Bischof, M. Bücker, P. Gibbon, G.R. Joubert, T. Lippert, B. Mohr,
F. Peters (Eds.),
John von Neumann Institute for Computing, Jülich,
NIC Series, Vol. **38**, ISBN 978-3-9810843-4-4, pp. 585-592, 2007.
Reprinted in: Advances in Parallel Computing, Volume **15**,
ISSN 0927-5452, ISBN 978-1-58603-796-3 (IOS Press), 2008.

http://www.fz-juelich.de/nic-series/volume38

Turbulence in Laterally Extended Systems

Jörg Schumacher[1] **and Matthias Pütz**[2]

[1] Department of Mechanical Engineering
Technische Universität Ilmenau
98684 Ilmenau, Germany
E-mail: joerg.schumacher@tu-ilmenau.de

[2] Deep Computing – Strategic Growth Business
IBM Deutschland GmbH
55131 Mainz, Germany
E-mail: mpuetz@de.ibm.com

We study three-dimensional turbulence in a very flat Cartesian cell with periodic boundaries in the lateral directions and free-slip boundaries in the vertical one. The pseudospectral simulations are conducted on the massively parallel Blue Gene/L system. The small amount of memory per core requires a two-dimensional parallelization of the numerical scheme. We report performance and scaling tests on up to 16384 CPUs and present first physical results for the case of convective turbulence.

1 Introduction

Turbulent flows appear frequently for lateral extensions that exceed the vertical ones by orders of magnitude. Examples can be found in planetary and stellar physics or in atmospheric and oceanographic science[1]. For example, atmospheric mesoscale layers or the Gulf stream evolve on characteristic lengths L of 500 - 5000 km in combination with vertical scales H of about 1 - 5 km. The resulting aspect ratios follow to $\Gamma = L/H = 100 - 1000$[1].

This is one main reason why many turbulence studies in geophysical context are conducted in two dimensions from beginning, i.e., the vertical variations of the fields under consideration are neglected. The description of the physical processes is done then only with respect to the remaining lateral coordinates (for a review see Ref. 2). However, the reduction of the space dimension from three to two alters the turbulence physics in a fundamental way. In three dimensions, kinetic energy is cascading from the largest eddies down to smaller ones. This regime is known as the *direct* cascade. In two dimensions, energy which is injected at small scales flows in an *inverse* cascade of the kinetic energy towards larger eddies. Such large-scale vortex structures are observed, e.g. as big storm systems or as the Red Spot on planet Jupiter. The reason for this cascade reversal is a topological one. The fundamental mechanism of vortex stretching which generates energy at finer scales is absent in two dimensions[2].

Theoretical studies on the crossover from three- to (quasi-)two-dimensional turbulence are rare. They are based on cascade models which are derived from the Fourier space formulation of the Navier-Stokes equations of motion. The space dimension d is included as a varying parameter. Fournier and Frisch[3] found a reversal of the turbulent energy cascade from direct to inverse when the space dimension becomes smaller than $d = 2.06$. Such crossover studies are not possible in a direct numerical simulation which uses a spatial

grid. However, one can extend a rectangular box in the two lateral directions successively while keeping the spectral resolution with respect to all three space coordinates the same. Theoretically, this allows for a horizontal rearrangement of flow structures on scales significantly larger than the vertical height of the cell. Turbulence can thus become quasi-two-dimensional for $\Gamma \gg 1$. The flat geometry will differently affect the turbulent transport of substances in the lateral directions compared to the vertical one. Frequently, such layers are in a state of convective turbulence that is caused by the temperature dependence of the fluid density. Furthermore, planets and stars rotate at constant angular frequencies, i.e. in addition to buoyancy effects Coriolis forces will appear[5]. This is exactly the system which we want to study. In the following, we describe preparatory steps for the implementation and first tests of the simulation program on the Blue Gene/L system.

2 Equations and Numerical Integration Scheme

The Boussinesq equations, i.e. the Navier-Stokes equations for an incompressible flow with an additional buoyancy term $\alpha g\theta \mathbf{e}_z$ and the advection-diffusion equation for the temperature field, are solved numerically for the three-dimensional case[6]. In addition, the Coriolis force term $2\Omega \mathbf{e}_z \times \mathbf{u}$ is added for cases with rotation about the vertical z-axis. The equations are then

$$\nabla \cdot \mathbf{u} = 0\,, \tag{2.1}$$

$$\frac{\partial \mathbf{u}}{\partial t} + (\mathbf{u}\cdot\nabla)\mathbf{u} = -\nabla p - 2\Omega \mathbf{e}_z \times \mathbf{u} + \nu\nabla^2\mathbf{u} + \alpha g\theta \mathbf{e}_z\,, \tag{2.2}$$

$$\frac{\partial \theta}{\partial t} + (\mathbf{u}\cdot\nabla)\theta = \kappa\nabla^2\theta + u_z\frac{\Delta T}{H}\,. \tag{2.3}$$

Here, $\mathbf{u}$ is the turbulent velocity field, p the pressure field and θ the temperature fluctuation field. The system parameters are: rotation frequency Ω, gravity acceleration g, kinematic viscosity ν, thermal diffusivity κ, aspect ratio $\Gamma = L/H$, vertical temperature gradient $\Delta T/H$, and thermal expansion coefficient α. The temperature field is decomposed into a linear mean profile (which causes the scalar driving term in (2.3)) and fluctuations θ

$$T(\mathbf{x},t) = -\frac{\Delta T}{H}(z - H/2) + \theta(\mathbf{x},t)\,. \tag{2.4}$$

Since T is prescribed at boundaries $z = 0$ and π, the condition $\theta = 0$ follows there. Here, $\Delta T > 0$. The dimensionless control parameters are the Prandtl number Pr, the Rayleigh number Ra, the Taylor number Ta, and the aspect ratio Γ,

$$Pr = \frac{\nu}{\kappa}\,, \quad Ra = \frac{\alpha g H^3 \Delta T}{\nu\kappa}\,, \quad Ta = \frac{4\Omega^2 H^4}{\nu^2}\,, \quad \Gamma = \frac{L}{H}\,. \tag{2.5}$$

The simulation domain is $V = L \times L \times H = [0, \Gamma\pi] \times [0, \Gamma\pi] \times [0, \pi]$. In lateral directions x and y, periodic boundary conditions are taken. In the vertical direction z, free-slip boundary conditions are used which are given by

$$u_z = \theta = 0 \quad \text{and} \quad \frac{\partial u_x}{\partial z} = \frac{\partial u_y}{\partial z} = 0\,. \tag{2.6}$$

The numerical method which is used is a pseudospectral scheme[7]. The partial differential equations of motion (2.1) – (2.3) are transformed to an infinite-dimensional system

of nonlinear ordinary differential equations in Fourier space. In a compact notation, the equations for a Fourier mode $\phi(\mathbf{k},t) = (u_i(\mathbf{k},t), \theta(\mathbf{k},t))$ and $\gamma = (\nu, \kappa)$ with a given wavevector $\mathbf{k}$ result then to

$$\frac{\partial \phi(\mathbf{k},t)}{\partial t} = -\gamma k^2 \phi(\mathbf{k},t) + F(\phi(\mathbf{q},t),t) \tag{2.7}$$

where the last term of (2.7) contains all mode couplings that arise due to the nonlinearity of the original equations. In order to avoid the explicit calculation of very large convolution sums, one transforms the respective terms into the physical space. Here, the products of the fields can be evaluated gridpointwise. The back- and forward transformations between physical and Fourier space are established by Fast Fourier Transformations (FFT) using the IBM-ESSL[8] or fftw[9] libraries.

The first term on the r.h.s. of (2.7) can be treated by the integrating factor. The substitutions $\tilde{\phi} = \exp(\gamma k^2 t)\phi$ and $\tilde{F} = \exp(\gamma k^2 t)F$ lead to

$$\frac{\partial \tilde{\phi}(\mathbf{k},t)}{\partial t} = \tilde{F}(\phi(\mathbf{q},t),t)\,. \tag{2.8}$$

This translates into the following second-order predictor-corrector scheme for the time integration[10]. We define the integrating factor $I_n = \exp(\gamma k^2 t_n)$. The predictor step is then given by

$$\phi^* = \frac{I_n}{I_{n+1}}[\phi_n + \Delta t F_n]\,. \tag{2.9}$$

The corrector step with $F^* = F(\phi^*)$ follows then to

$$\phi_{n+1} = \frac{I_n}{I_{n+1}}\left[\phi_n + \frac{\Delta t}{2}F_n\right] + \frac{\Delta t}{2}F^*\,. \tag{2.10}$$

3 3D-FFT Packages for Blue Gene/L

One of the main building blocks of the present numerical method is the Fast Fourier Transform (FFT). The classical parallel implementation of three-dimensional FFTs uses a slabwise decomposition of the simulation domain. For a simulation with N^3 grid points, the method allows a parallelization on up to N processors. Due to the rather small memory size per core, the Blue Gene/L requires a *volumetric* FFT which decomposes the three-dimensional volume into so-called pencils and hence allows a parallelization degree of N^2. The prime requirement for being able to run a simulation with a large grid is that the domain fractions of the grid (including buffers and temporary storage) fit into the 512 MB of memory on a single Blue Gene/L node. At same time, of course, the FFT algorithm should also be scalable, i.e. increasing the number of CPUs to solve the problem should also substantially decrease the time-to-answer.

To check this we compared[11] three FFT packages on a small test case: the old slabwise method, the BGL3DFFT package by M. Eleftheriou *et al.*[12] and the P3DFFT package by D. Pekurovsky[13]. The second package is written in C++ and contains complex-to-complex FFTs only (Fortran- and C-bindings are available from IBM). The first and third package are available in Fortran. The results on strong scaling are summarized in Fig. 1. For the

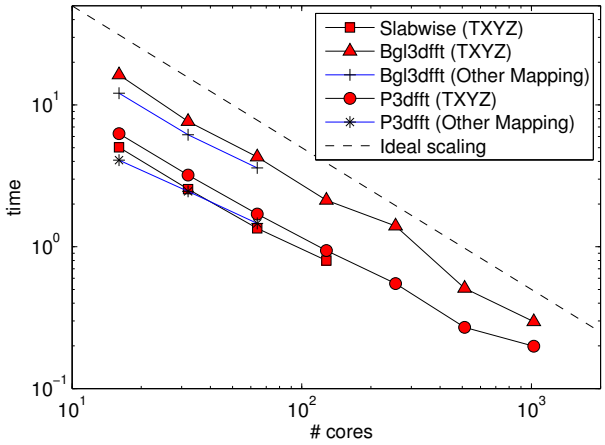

Figure 1. Strong scaling tests for the three different FFT packages on up to 1024 cores. The test function is $f(x, y, z) = \sin(x)\cos(2y)\sin(z)$ which is resolved on an equidistant 128^3 cubic grid of side length 2π. Other mapping means that we have edited map files by hand.

volumetric FFT packages, we have varied the mapping of the MPI tasks onto the torus grid network of Blue Gene/L . By default, Blue Gene/L maps MPI tasks on all primary cores of a partition first, i.e. the corresponding environment variable is set to `BGLMPI_MAPPING = XYZT`. Beside the fact that the P3DFFT interface and implementation supports our needs in an optimal way (real-to-complex/complex-to-real FFTs), it also turned out to be the best solution in terms of performance. For example, the symmetry $\mathbf{u}(\mathbf{k}) = \mathbf{u}^*(-\mathbf{k})$ for real-to-complex transforms is explicitely implemented already. Additionally, the in-place transformation flag allows the storage of physical and Fourier space fields in the same array.

4 Simulation Results

4.1 Scaling Rests on Blue Gene/L

The strong scaling of the whole simulation code is shown in Fig. 2 for 16 to 2048 cores. The resolution is $512 \times 512 \times 64$ grid points with an aspect ratio $\Gamma = L/H = 16$. All tests have been done in the virtual node (VN) mode. For more than 256 cores the `mpirun` option for the processor topology, `BGLMPI_MAPPING = XYZT`, brought the shortest computation times. The analysis of the code with the `mpitracelib` indicated that after these steps had been made almost all of the communication overhead remained in the `MPI_alltoallv` communication task which is required in the FFT algorithm for the transposition of the pencils. Hence it is the only factor which limits strong scaling on a larger number of cores eventually. Future improvements of the implementation of `MPI_alltoallv` will therefore have an immediate impact on the performance of our code.

Table 1 summarizes our findings for grid resolutions in production runs, i.e. $N_x \times N_y \times N_z = 4096 \times 4096 \times 256$ at $\Gamma = 32$. For such large grids it became necessary to implement

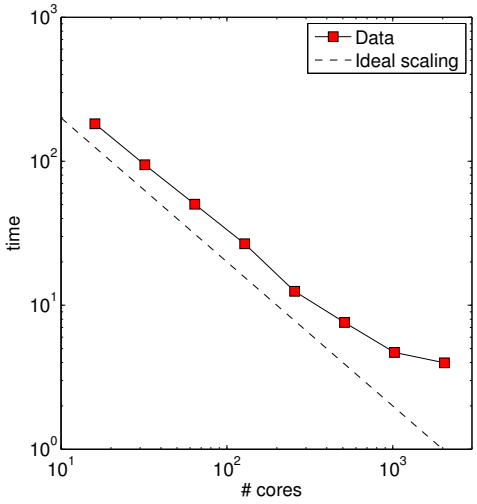

Figure 2. Strong scaling test for the code from 16 to 2048 CPUs cores. Note that the computational volume for this test case is a very flat cell with an aspect ratio of $\Gamma = 16$.

some internal summation loops in double precision. All of these loops appear in the calculation of the right-hand-side of the equations of motion which is the most expensive part of the program. The number of grid points per MPI task was of the order of 10^6 which is simply too large to sum over with 32-bit floating point precision. We have studied the two

# tasks	2048	1024	4096	4096	8192	4096	16384	8192	8192
Mode	VN	CO	VN	VN	VN	CO	VN	CO	VN
$iproc$	32	32	64	128	128	64	128	128	512
$jproc$	64	32	64	32	64	64	128	64	16
time(s)	183.3	205.7	118.6	109.6	77.8	90.66	62.6	60.5	74.0

Table 1. Runtime tests for the run with an aspect ratio $\Gamma = 32$. The CPU time was measured with the MPI_Wtime() task for a loop of 5 integration steps.

modes of the dual core chip, the virtual node mode (VN) and the co-processor mode (CO). The parameters $iproc$ and $jproc$ in the table represent the two dimensions of the processor grid that has to be generated for the volumetric FFTs. Note, that the ratio $iproc/jproc$ can be tuned as long as $iproc \times jproc = N_{core}$. In general, a ratio of one would be best, but other choices can be better, if they improve the mapping of the MPI tasks onto the partition grid. For the large problem we observe that the differences between the VN and CO modes are small. This is due to the fact that large local grid fractions do no longer fit into the L3 cache of a Blue Gene/L node and have to be streamed from memory. If the second core is used for computation (VN mode) the two cores are actually competing for the memory bandwidth of the node and the gain in computing time is fairly small. The

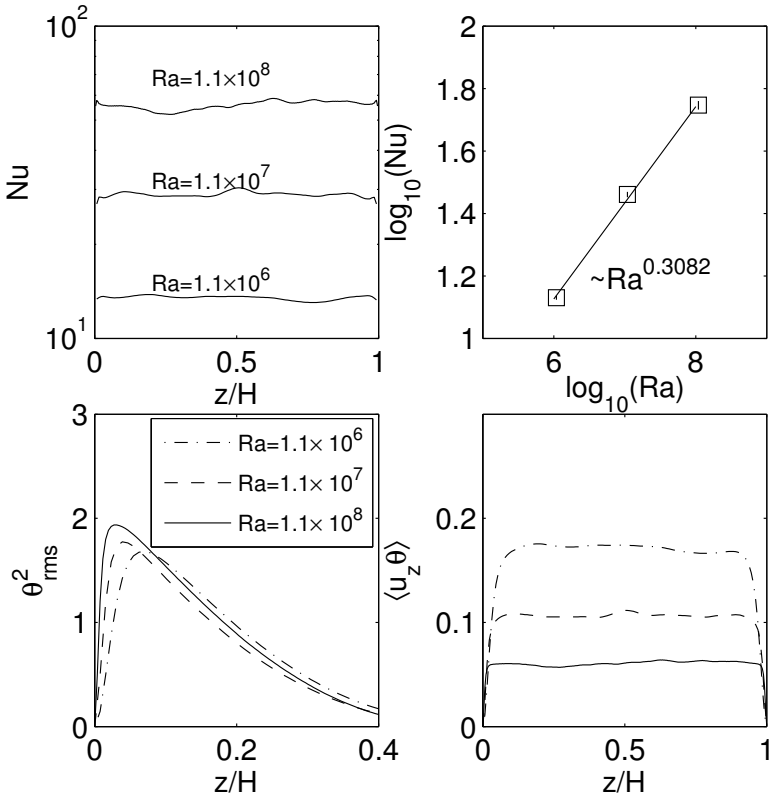

Figure 3. Turbulent heat transport in convective turbulence. Left upper panel: Vertical profiles $Nu(z)$ for three runs. The mid line is the Blue Gene/L run. Upper right panel: Nusselt number scaling with respect to Ra. The resulting scaling exponent is also indicated in the figure. Lower left panel: Vertical profiles of the mean square temperature fluctuations. Lower right panel: Vertical profiles of the mixed turbulent stress $\langle u_z \theta \rangle$. Linestyles are the same as in the lower left panel.

communication time in VN mode is however bigger than in CO mode, such that these two effects almost compensate each other. The table indicates that the runtime starts to saturate for $N_{core} \geq 8192$. There is no chance to improve the cache locality of the code to avoid this, because the FFTs will always require the full grid. There may however be some further optimization potential by using explicit task mappings. The main problem here is to find an embedding of a 2d grid decomposition into a 3d torus communication grid, such that no communication hot spots occur on the point-to-point network of the Blue Gene/L. In general, this is a hard problem.

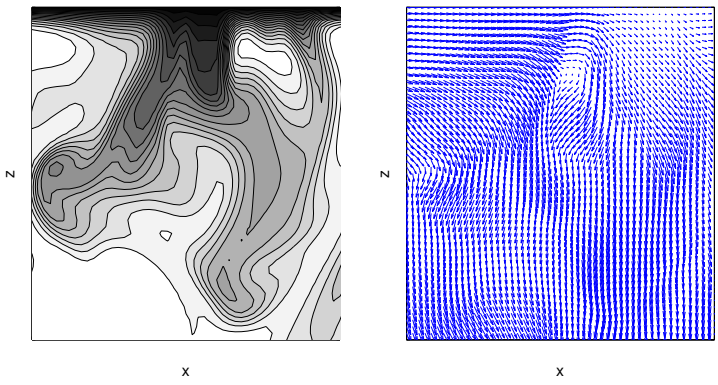

Figure 4. Magnification of a small fraction of the vertical cut through the three-dimensional volume at $y = \pi$. The region in the vicinity of the cold top plane is shown for a simulation at $Ra = 1.1 \times 10^8$. Left panel: Full temperature field T. Right panel: Corresponding velocity field (u_x, u_z). The figures illustrate a cold finger-like plume which falls down into the turbulent bulk and the corresponding fluid motion.

4.2 Comparison of First Physical Results

First physical results for convective turbulence without rotation are presented now for an aspect ratio $\Gamma = 2$. The simulation was conducted at $Ra = 1.1 \times 10^7$ and $Pr = 0.7$. The results are compared with former simulation runs in the same parameter range and for the same Γ. The resolution for this benchmark run is $N_x \times N_y \times N_z = 256 \times 256 \times 256$. It was run on 32 cores. Figure 3 presents our results for the turbulent heat transport, the mean square fluctuations of the temperature field and the mixed turbulent stress of temperature and vertical velocity. The turbulent heat transport is given by the dimensionless Nusselt number Nu which is defined as

$$Nu(z) = \frac{\langle u_z \theta \rangle_A - \kappa \partial \langle T \rangle_A / \partial z}{\kappa \Delta T / H}, \tag{4.1}$$

where $\langle \cdot \rangle_A$ denotes an statistical average over lateral $x - y$ planes. The upper left panel of Fig. 3 demonstrates that the relation $Nu(z) = const.$ holds approximately for all cases. The mean of $Nu(z)$ over z is Nu which is shown as a function of the Rayleigh number in the upper right panel. The algebraic scaling $Nu \sim Ra^{0.31}$ corresponds with findings from other simulations. The vertical profiles of the mean square temperature fluctuations are shown in the lower left panel. The distance of the maximum of the profile to the free-slip wall corresponds with the thermal boundary layer thickness. It decreases with increasing Ra and puts thus stronger resolution requirements on the simulation. The lower right panel shows the turbulent stress $\langle u_z \theta \rangle$. The turbulence becomes homogeneous for the lateral planes that form the plateau in the profiles. We also found that very long time series are necessary for a satisfactory turbulence statistics. The reason for a long time series lies in coherent structures that are formed in the vicinity of both free-slip planes as shown in Fig. 4. They go in line with strong local correlations between the fluctuating temperature field and the turbulent vertical velocity component. To summarize, the results of the BG/L test run fit consistently into the former studies.

5 Concluding Remarks

Significant efforts had to be taken in order to port the pseudospectral turbulence simulation code on the massively parallel Blue Gene/L system, including the switch to fast Fourier transformations that are parallelized in two dimensions. Two factors are coming together in our problem: the small amount of memory per core and the very flat geometry that causes strongly asymmetric pencils in the domain decomposition. The use of the P3DFFT package and a number of changes in the communication overhead improved the performance of the code on the Blue Gene/L system significantly and provide now a basis for further studies of turbulence in this specific flat geometry. The latter is of interest for many geophysical and astrophysical problems.

Acknowledgements

JS wishes to thank the John von Neumann-Institute for Computing for their steady support with supercomputing ressources. We thank J.C. Bowman, R. Grauer, D. Pekurovsky and P.K. Yeung for helpful discussions. This work is supported by the Deutsche Forschungsgemeinschaft under Grant No. SCHU/1410-2.

References

1. B. Cushman-Roisin, *Introduction to Geophysical Fluid Dynamics*, (Prentice Hall, Englewood Cliffs, NJ, 1994).
2. P. Tabeling, *Two-dimensional turbulence: a physicist approach*, Phys. Rep., **362**, 1–62, (2002).
3. J.-D. Fournier and U. Frisch, *d-dimensional turbulence*, Phys. Rev. A, **17**, 747–762, (1978).
4. L. P. Kadanoff, *Turbulent heat flow: structures and scaling*, Phys. Today, **54**, 34–39, (2001).
5. K. Julien, S. Legg, J. C. McWilliams and J. Werne, *Rapidly rotating turbulent Rayleigh-Benard convection*, J. Fluid Mech., **322**, 243–273, (1996).
6. J. Schumacher, K. R. Sreenivasan and V. Yakhot, *Asymptotic exponents from low-Reynolds-number flows*, New J. Phys., **9**, art. no. 89, (2007).
7. C. Canuto, M. Y. Hussaini, A. Quarteroni and T. A. Zang, *Spectral Methods Methods in Fluid Dynamics*, (Springer, Berlin, 1988).
8. `http://www.www.ibm.com/systems/p/software/essl.html`
9. `http://www.fftw.org/`
10. P. K. Yeung and S. B. Pope, *An algorithm for tracking fluid particles in numerical simulations of homogeneous turbulence*, J. Comp. Phys., **79**, 373-416, (1988).
11. J. Schumacher and M. Pütz, *Report on the Blue Gene/L Scaling Workshop 2006*, Editors: W. Frings, M.-A. Hermanns, B. Mohr and B. Orth, Technical Report FZJ-ZAM-IB-2007-02, , 15–18, (2007).
12. M. Eleftheriou, B. G. Fitch, A. Rayshubskiy, T. J. C. Ward, and R. S. Germain, *Scalable framework for 3D FFTs on the Blue Gene/L supercomputer: implementation and early performance measurements*, IBM J. Res. & Dev., **49**, 457–464, (2005).
13. `http://www.sdsc.edu/us/ressources/p3dfft.php`